Journal of Asian Earth Sciences 92 (2014) 224–232

Contents lists available at ScienceDirect

Journal of Asian Earth Sciences

journal homepage: www.elsevier.com/locate/jseaes

Marine controlled source electromagnetic method used for the gas hydrate investigation in the offshore area of SW Taiwan

Shu-Kun Hsu [a,*], Chih-Wen Chiang [b], Rob L. Evans [c], Chow-Son Chen [a], Shye-Donq Chiu [d], Yu-Fang Ma [d], Song-Chuen Chen [e], Ching-Hui Tsai [a], Shiao-Shan Lin [a], Yunshuen Wang [e]

[a] Department of Earth Sciences, National Central University, Taiwan
[b] Institute of Applied Geosciences, National Taiwan Ocean University, Taiwan
[c] Department of Geology and Geophysics, Woods Hole Oceanographic Institution, USA
[d] Institute of Oceanography, National Taiwan University, Taiwan
[e] Central Geological Survey, Ministry of Economic Affairs, Taiwan

ARTICLE INFO

Article history:
Received 8 February 2013
Received in revised form 23 November 2013
Accepted 1 December 2013
Available online 14 December 2013

Keywords:
Gas hydrate
EM method
Gas seepage
Pockmark
SW Taiwan

ABSTRACT

Bottom simulating reflectors (BSRs), high methane flux, shallow sulfide/methane interfaces, fluids venting from the seafloor, authigenic carbonates within sediments, methane reefs, and self-biomes are common seafloor features in the area off southwest Taiwan. The geophysical and geochemical signatures of these features suggest a high potential for gas hydrate (GH) reservoirs in the region. The BSRs are typically interpreted as the boundary between free gases and solid hydrate, whereas the upper reaches of the hydrate stability zone and the distribution of gas hydrate in shallow sediments are not well understood. This study shows the first results of a marine controlled-source electromagnetic survey, conducted in the offshore area of SW Taiwan in 2010. The survey aimed to provide electrical resistivity information of the shallow sediments. Three target areas were surveyed: (1) an area to the southeast of the Xiaoliuchiu Island (gas seep G96), (2) an area in the west of the Yung-An Ridge (YAR) and (3) an area in the northwest of the Good Weather Ridge (GWR). In total, fourteen survey lines with a total length of 72 km were completed. Our preliminary results show that relatively high resistivity anomalies occur within pockmarks and at gas seepage sites. The apparent resistivity is estimated to be about 1 Ohm-m higher than background in G96 and YAR sites, while an anomaly up to 2 Ohm-m is found in the GWR. At gas seep site G96, the high resistivity anomaly may be due to the existence of authigenic carbonates; whereas, the high resistivity anomaly in the NW of the GWR site may also be due to the existence of gas hydrate in the shallow seabed. Based on the resistivity anomaly, the gas hydrate saturation is about 16% in the shallow sediments below the pockmark area in the northwest side of the GWR site.

1. Introduction

A widespread distribution of bottom simulating reflectors (BSRs) (Chi et al., 1998; Liu et al., 2006), high methane concentrations in the bottom water (Chuang et al., 2006), a shallow sulfate/methane interface (Lin et al., 2006), active methane venting from submarine mud volcanoes (Hsu et al., 2013), mud diapirs and gas seepages (Chen et al., 2010) in the offshore area of southwest Taiwan all suggest a high potential of gas hydrates resources. However, crystallized methane hydrate (MH) has not yet been observed in over 60 piston core samples, including 4 giant piston cores by R/V *Marion Dufresne* (Liu et al., 2006).

BSRs from marine seismic reflection surveys are generally linked to the occurrence of MH-bearing formations. The presence of BSRs is typically interpreted to correspond to the base of the hydrate stability (BGHS) zone, marking a boundary between free gases and the solid hydrates. Thus, the BSR might be used as an indicator of a methane hydrate (MH) deposit. As a matter of fact, the BSR is a better indication of the existence of free gas beneath the BGHS (Paull and Ussler, 2001).

The upper boundary of the hydrate stability zone is poorly understood and is greatly influenced by fluid advection (e.g. Xu and Ruppel, 1999). In convergent margin settings, fluid flux is especially high as a result of the squeezing of sediments, resulting in mud volcanoes (Milkov, 2000) and other gas seepage systems. Important chemical fluxes of methane (e.g. Hovland and Judd, 1988; Hovland et al., 1993) and groundwater in coastal settings also pass through shallow sediments into the ocean. Thus, the upper bound of MH in shallow sediments still remains uncertain in areas where hydrate potential is only based on the location of a BSR (e.g. Liu et al., 2006).

* Corresponding author. Tel.: +886 3 4268316; fax: +886 3 4222044.
E-mail address: hsu@ncu.edu.tw (S.-K. Hsu).

1367-9120/$ - see front matter © 2013 Elsevier Ltd. All rights reserved.
http://dx.doi.org/10.1016/j.jseaes.2013.12.001

Because the gas hydrate is generally associated with high resistivity, marine electromagnetic techniques are considered to be an effective way to image gas hydrates (GH) in the shallow portion of the seabed (Edwards, 1997; Evans, 2007; Ellis et al., 2008; Goto et al., 2008; Schwalenberg et al., 2010; Chiang et al., 2011, 2012; Weitemeyer et al., 2011). We therefore carried out the first marine controlled source electromagnetic (MCSEM) survey off southwest Taiwan in order to better understand the potential gas hydrate in this region (Fig. 1).

2. Data acquisition and processing

In order to image the shallow section of sediment, we use a towed electromagnetic (EM) system manufactured by Woods Hole Oceanographic Institution (Evans, 2007). The towed EM system is a frequency-domain, magnetic dipole–dipole array (Fig. 2). The system is composed of 3 receivers and a transmitter forming an array with a total length of ~40 m on the seafloor. The system is pulled along the seafloor at speeds of 1–2 knots. The 3 receivers are

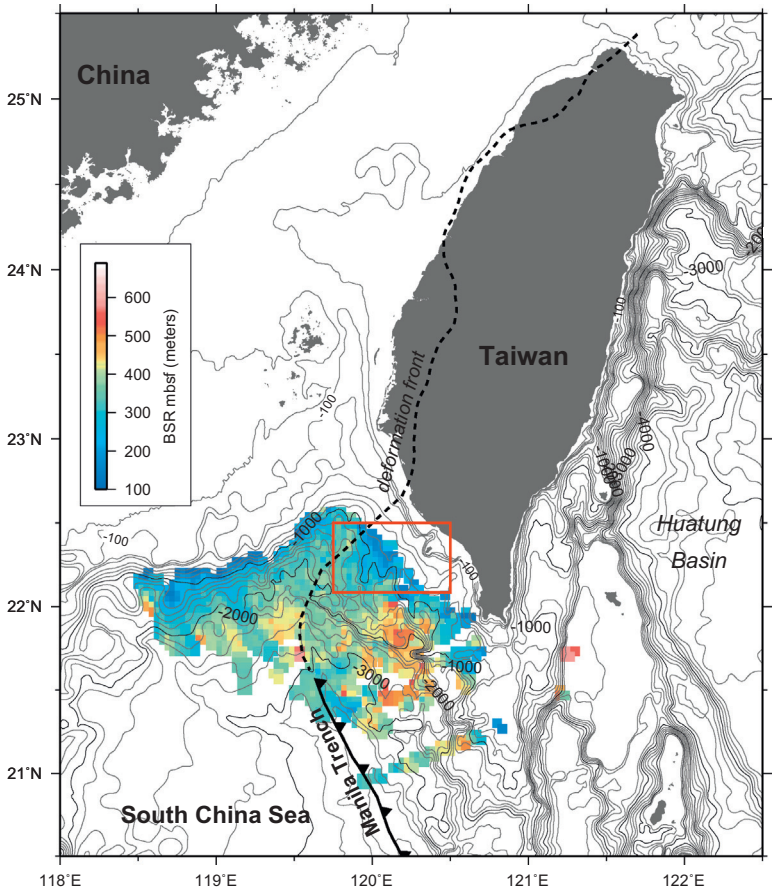

Fig. 1. The BSR distribution off SW Taiwan is superposed on the bathymetry. The red box indicates the study area. mbsf: meters below sea floor. (For interpretation of the references to colour in this figure legend, the reader is referred to the web version of this article.)

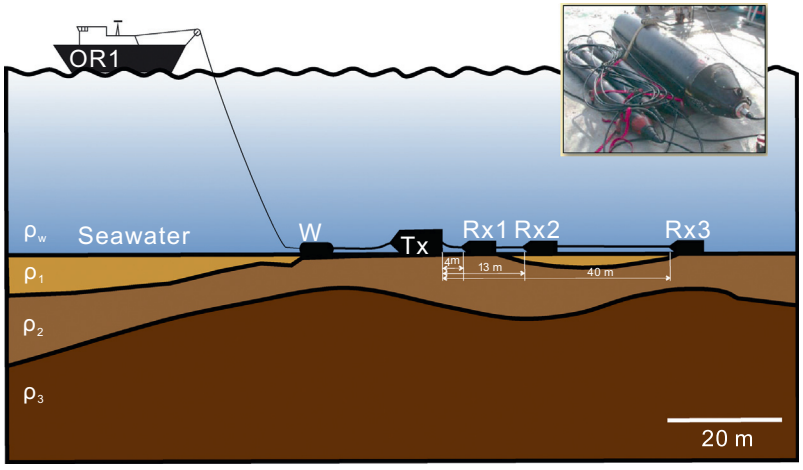

Fig. 2. Schematic configuration of towed EM system (modified from Evans et al., 1999). *W*: a weight as a depressor unit; *Tx*: transmitter; σ: conductivity. Rx1, Rx2 and Rx3 and three different receivers. Up-right panel shows the real instruments.

spaced at 4 m, 13 m and 40 m behind the transmitter. Each receiver measures the inline component of the magnetic field amplitudes and phases at 3 different frequencies ranging from 200 Hz to 200 kHz. The system is controlled and powered by a computer and power-supply on-board ship. Data are telemetered through the conducting tow cable and logged in real-time. Each cycle of measurement for all the three receivers takes about 20 s to complete data acquisition. The sampling interval is roughly every 10–20 m along the seafloor, while the instrument is continually at 1–2 knots. More details of the system can be found in Evans (2007).

Our study area is located in the northern end of the Manila subduction zone where the Eurasian Plate is subducting eastward beneath the Philippine Sea Plate, and is also located in the junction area between the Chinese passive continental margin and the active accretionary wedge (Sibuet and Hsu, 2004; Liu et al., 2004, 1997) (Fig. 1). In order to obtain electrical parameters of shallow

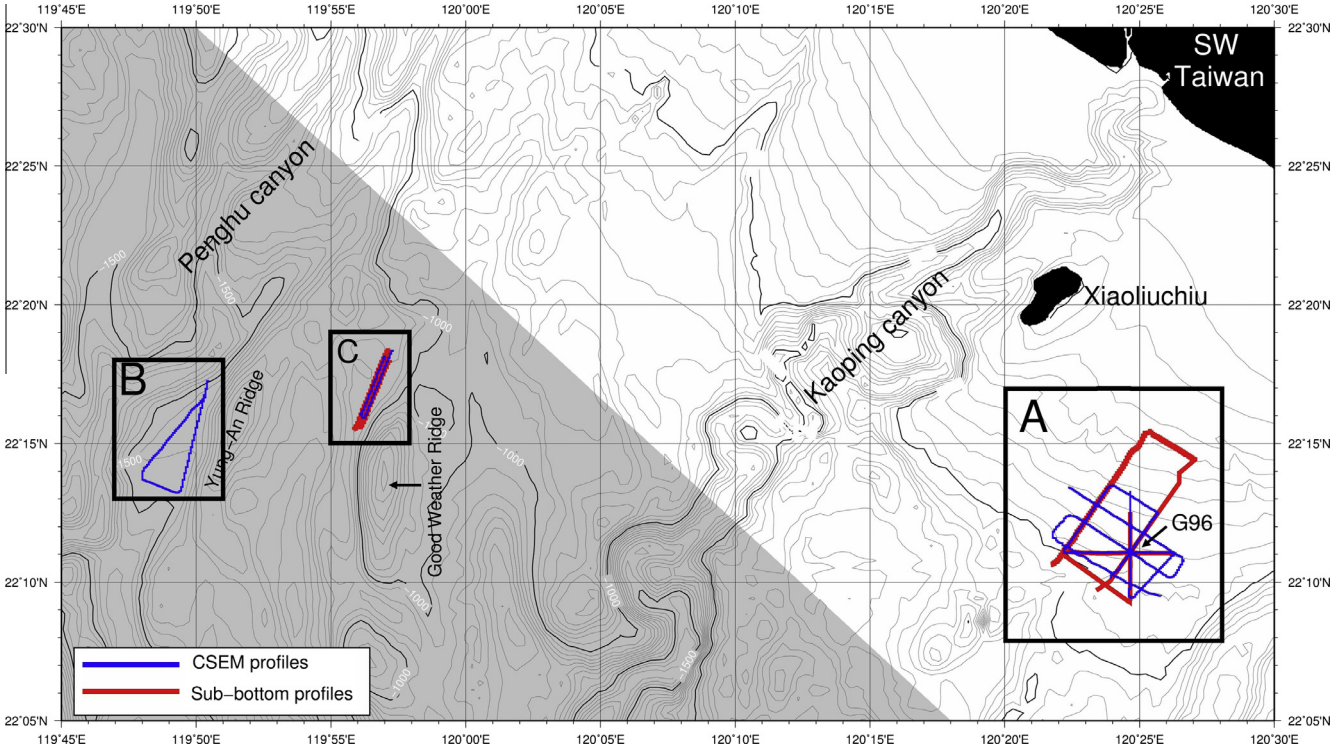

Fig. 3. Detailed bathymetry of three study areas. The gray area indicates that BSR is generally observed beneath the gray area. A: gas seepage G96 area. B: an area in the west of the Yung-An Ridge. C: an area in the northwest of the Good Weather Ridge.

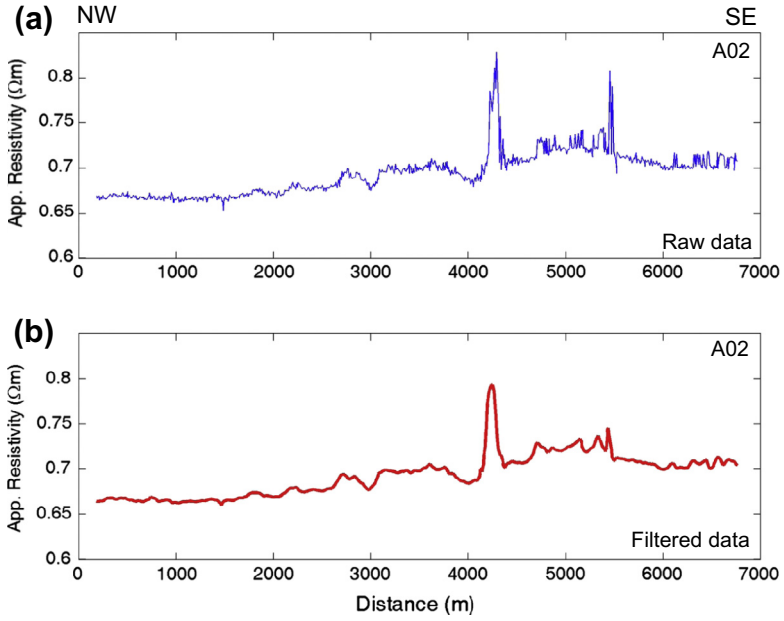

Fig. 4. Example of a smoothing process along profile A02. (a) The collected raw data and (b) the data has been smoothed with a Butterworth filter.

sediments to better understand the potential of MH reservoirs, three target areas were chosen on the basis of the existing geophysical data: (1) southeast of the Xialiuchiu Islands (or gas seepage, G96), (2) west of the Yung-An Ridge (YAR) and (3) northwest of the Good Weather Ridge (GWR) (Fig. 3).

Our MCSEM survey was conducted during cruise ORI-931 on board R/V Ocean Researcher I in June 2010. The total survey length is about 72 km with 14 profiles collected (Fig. 3). Unfortunately, a failure of optical fiber connection (modems) occurred and caused a malfunction of the 4 m and 40 m receivers. Thus, we only have data from the receiver at 13 m behind the transmitter. Raw data are displayed as apparent resistivity values. Because we only have measurements at a single source-receiver offset, we are unable to constrain vertical gradients in resistivity. Thus, an apparent resistivity is an average over the top ~6.5 m (half the source-receiver offset) (Evans, 2001). Even so, we can observe the resistivity anomalies associated with the gas seep and pockmark features identified from the sub-bottom profiles and the Simrad EK500 sonar images.

To obtain an apparent porosity related to the apparent resistivity of the EM data, we use a modified form of the Archie's empirical equation (Archie, 1942):

$$\rho_f = A\rho_w\phi^{-m}, \tag{1}$$

where ϕ is the sediment apparent porosity; ρ_f is the apparent resistivity of the measured formation; ρ_w is the resistivity of seawater and can be derived from a CTD sensor; m is the cementation factor, and A is a constant. Typically the value m is between 1.4 and 2 for marine sediment samples (Jackson et al., 1978). Parameter A is the - fluid saturation. Here, we set $A = 1$ (assuming complete saturation) and $m = 1.8$ (Evans et al., 1999). Typical values of ρ_w are between

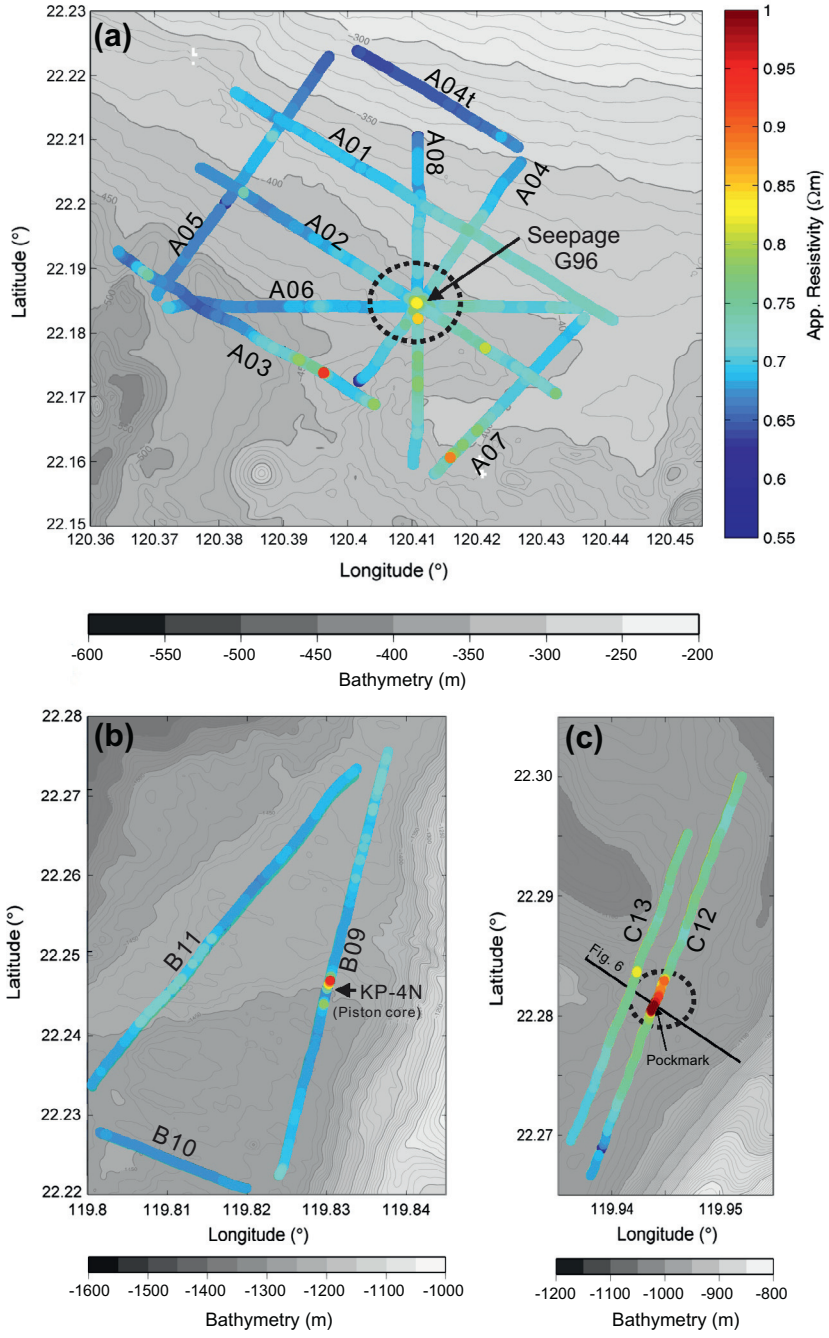

Fig. 5. Spatial distribution of the apparent resistivities along survey tracks (a) Along-track resistivities in area A, (b) Along-track resistivities in area B, and (c) Along-track resistivities in area C. A sub-bottom profiler and sidescan sonar images showing the pockmark in profile C12 are plotted in Fig. 6.

0.28 and 0.33 Ohm-m for normal seawater near the seafloor. The apparent porosity curve can be treated as a time series. High frequency noise could be due to very short wavelength bathymetric relief. Thus, we used a band-pass Butterworth filter between 1e-5 and 5 Hz to smooth the apparent resistivity curves and remove the effects of outliers (Butterworth, 1930) (Fig. 4).

3. Apparent resistivity and porosity anomalies at gas seep and pockmark areas

The measured apparent resistivity distribution along the survey tracks is shown in Fig. 5a–c. In survey area A, the CSEM profiles crossed gas seep site G96 (Fig. 5a). As shown by the sub-bottom profiler and side-scan sonar image, CSEM profile C12 passed through a pockmark near the convergent thrust at the western foot of the GWR (Fig. 6). Taking into account the seawater resistivity, the survey area A has generally the lowest apparent porosities (Fig. 7). Furthermore, the apparent resistivity at gas seep site G96 is ~0.1 Ohm-m higher than the surrounding area (Fig. 8), which corresponds to ~4% lower apparent porosity than the surrounding area. Relatively high resistivity anomalies also appear at gas seep site G96 along profiles A04, A06 or A08 (Figs. 5a and 8). Furthermore, apparent resistivities at crossing points of the profiles are coherent thus giving weight to the repeatability and confidence in the measurement. This shows that the measurements are repeatable and credible. In area A, the relatively high resistivity values are generally distributed in the southeast (Fig. 5a). Because area A is generally at a seawater depth not favorable for gas hydrate formation (Fig. 3), free methane migrates upward through gas seep site G96. Thus, the relatively high apparent resistivity at gas seep site G96 may be due to the existence of the authigenic carbonates beneath the shallow sediments or due to a larger quantity of free gas. In area B, a large resistivity anomaly occurs in the middle of profile B09 where a drilling site KP-4 N was proposed on the basis of seismic reflection profiles (Figs. 5b and 9a) (Liu et al., 2006). There is no significant resistivity anomaly along profiles B10 and B11. The reason for the resistivity anomaly needs to be examined in the future. In area C, an obvious resistivity anomaly of ~0.2 Ohm-m appears in the middle of profile C12, corresponding to a pockmark area (Figs. 5c, 6 and 10a). In contrast, there is only a slightly higher resistivity at the location close to the pockmark in profile C13 (Figs. 5c and 10b). However, the high resistivity anomaly in profile C12 does not appear exactly above the pockmark. Instead, it appears at the flank of the pockmark. One possibility is that the main gas hydrate is distributed beneath the flank rather than beneath the central pockmark depression.

The statistics of all the calculated apparent porosities in our study areas are shown in Fig. 7e–h. The apparent porosities range from 51% to 73%. For the profiles in area A, the apparent porosities range from about 51% to 68%, for the profiles in area B the apparent porosities range from 61% to 73%, and for the profiles in area C the apparent porosities range from 52% to 65%. The average of the apparent porosities is lowest in area A (Fig. 7e–h). Both the geologic setting and the salinity of seawater are important factors for estimating the porosity values (e.g. Hoefel and Evans, 2001; Evans and Lizarralde, 2011). In our case, the lower seawater resistivity in area A has derived a lower apparent porosity (cf. Fig. 7d and h). In real data samples, some sediment cores near N22°13.57′ and E119°57.07′ at water depth around 570 m show the sediment porosities between 35% and 55% (Jiang et al., 2006). If that is similar to our study area, our estimation of the apparent porosities is about 20% larger than the calculation from the core samples of Jiang et al. (2006). In that case, the parameter m in Eq. (1) may be 1.9 for the area off SW Taiwan.

The apparent resistivity values of profiles A02 and A06 in area A are compared to the corresponding sub-bottom profiles and EK500 sonar images (Fig. 8). The relatively high resistivity anomaly at the G96 seepage structure is consistent with the gas plume feature in the seawater column. Because the G96 site is located at a place where no BSR is observed (Fig. 3), the high resistivity anomaly at shallow depth of the seabed may be ascribed to the focused gas in the sediments. In area B, a significant high resistivity anomaly exists near site KP-4 N in profile B09. The core KP-4 N is located at the footwall of a convergent thrust fault to the west of the YAR anticline and is mainly composed of mud (Lin, 2010). Although

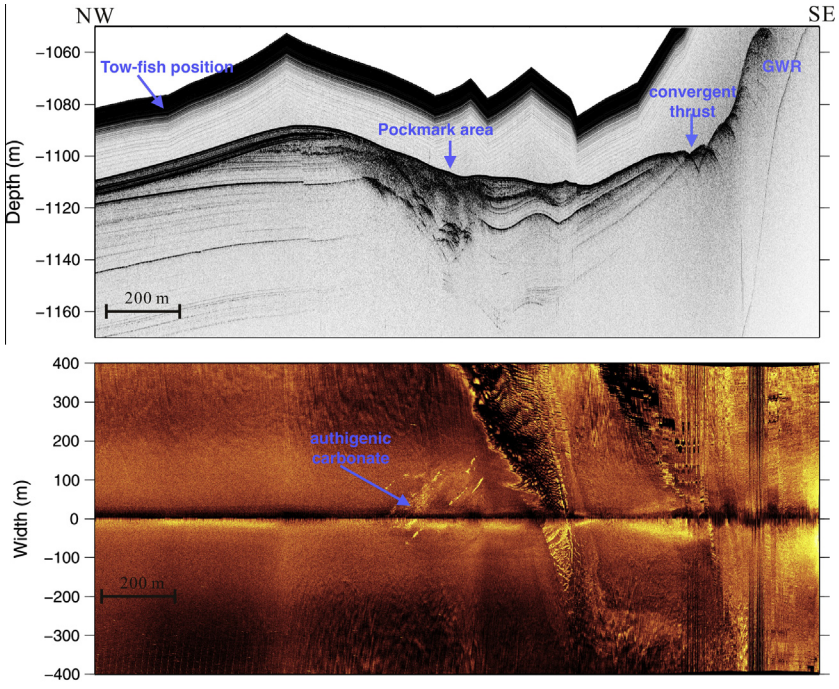

Fig. 6. A deep-tow sub-bottom profile (above panel) and side-scan sonar image (lower panel) collected along a profile that cuts across the pockmark shown in Fig. 5c. GWR: Good Weather Ridge. The bright yellow color in the side-scan image represents a strong backscatter intensity. (For interpretation of the references to color in this figure legend, the reader is referred to the web version of this article.)

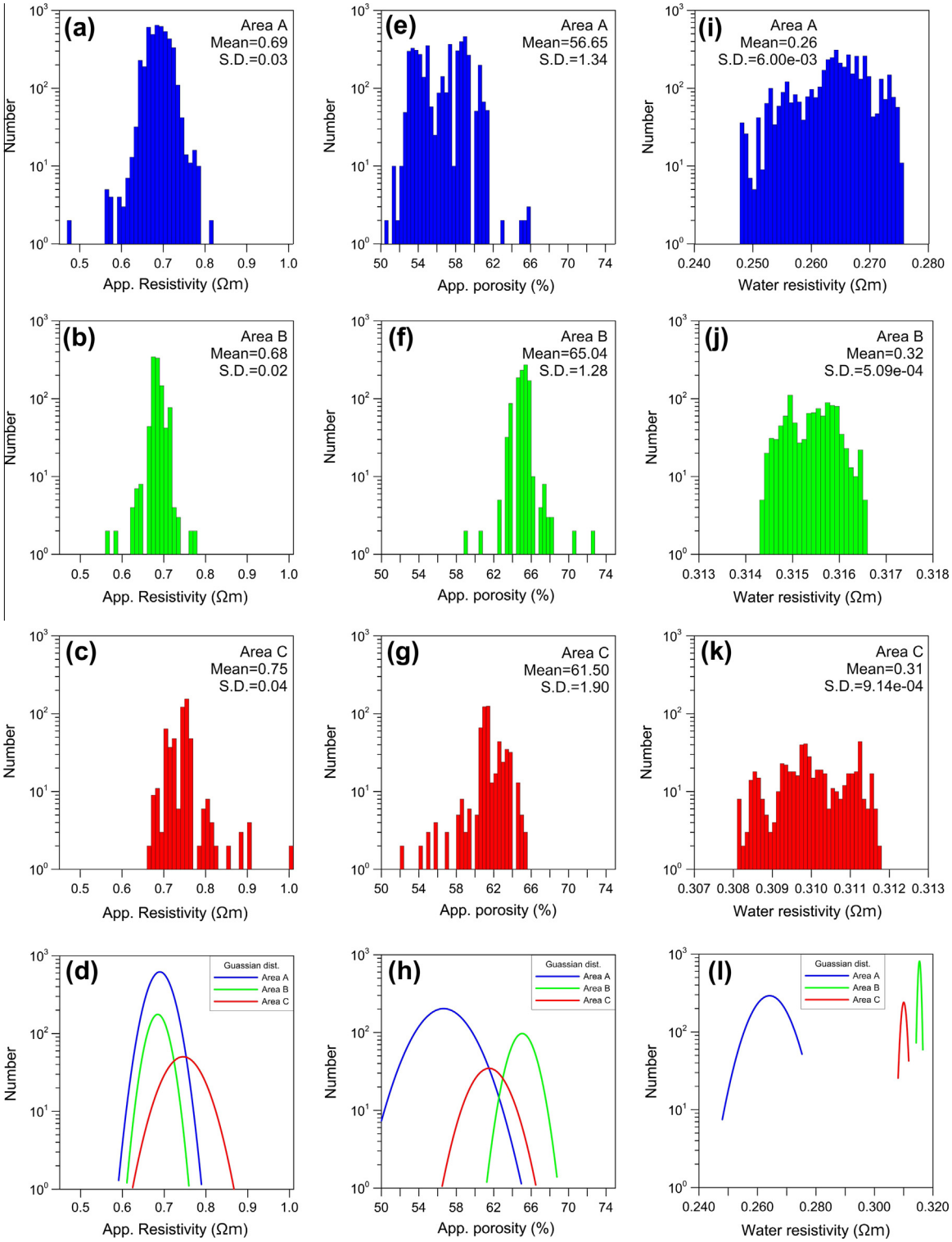

Fig. 7. The statistics of the apparent resistivities (in panels a, b and c), apparent porosities (in panels e, f and g) and seawater resistivities (in panel i, j and k) in survey areas A, B and C, respectively. Panels d, h and l show the Gaussian distributions of the apparent resistivities, apparent porosities and seawater resistivities of the three different areas.

there is no corresponding gas plume feature in the seawater, there is a depressed seabed feature. The most interesting feature related to gas hydrates appears in area C and is associated with a pockmark structure (Figs. 5, 6 and 10). The tectonic contexts for profile C12 and B09 are quite similar and both are located near a convergent thrust (Fig. 2). The resistivity anomaly is about 0.25 Ohm-m in profile C12, which is about a 33% increase with respect to the background resistivity.

4. Estimation of the gas-hydrate saturation beneath the pockmark area in the NW of the Good Weather Ridge

Based on ambient pressure–temperature conditions and the presence of a BSR indicator (Fig. 3) (Liu et al., 2006), the location of the lowest apparent porosity (~52%) in the middle of profile C12 very likely contains gas hydrate (Fig. 10). If gas hydrate is present, Eq. (1) can be generalized to

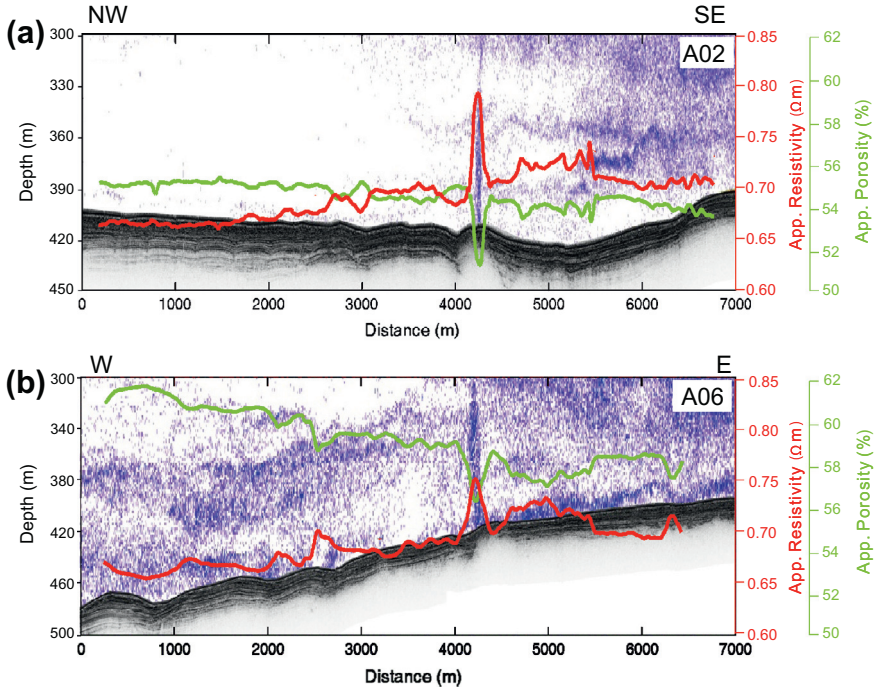

Fig. 8. Comparison between apparent resistivity or apparent porosity values and the sub-bottom profiler images along profiles A02 (a) and A06 (b), respectively. The pseudo-color images of a 38 kHz EK500 acoustic sounder are plotted above the sub-bottom profilers. It is noted that a gas plume (or a gas flare) with stronger reflectance (purple color) is observed above the gas seep site G96, where the apparent resistivity of the shallow sediments is about 0.1 Ohm-m higher than the background. (For interpretation of the references to color in this figure legend, the reader is referred to the web version of this article.)

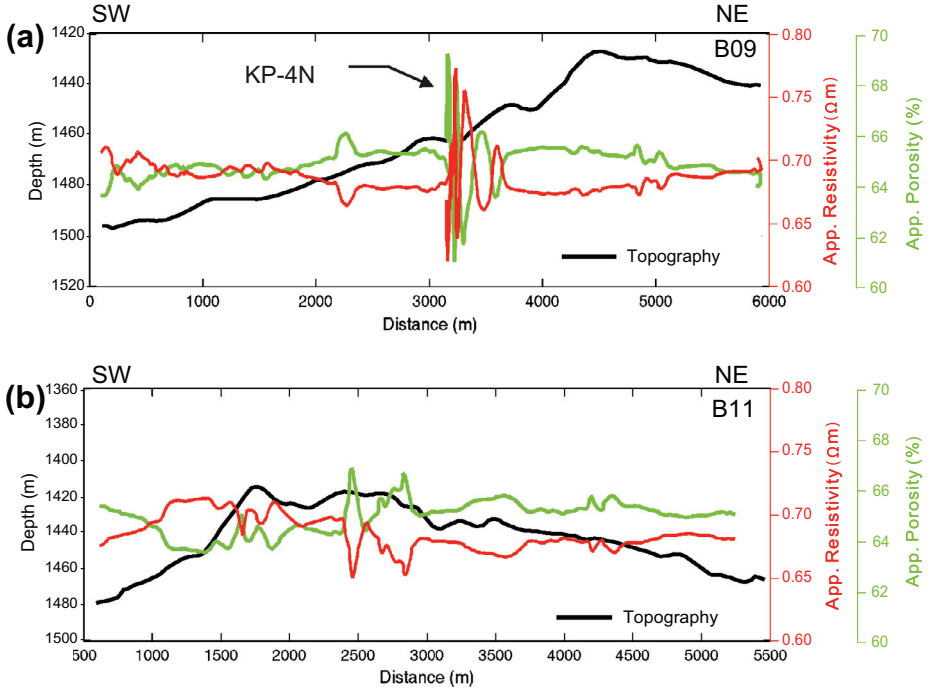

Fig. 9. Comparison between apparent resistivity or porosity values and seabed morphology measured in area B. (a) For profile B09, and (b) for profile B11.

$$\rho_f = A\rho_w S_w^{-n}\phi^{-m} \quad (2)$$

where S_w is the pore water saturation factor, n is the saturation coefficient and is often equal to m. $S_h = (1 - S_w)$ is the fractional gas hydrate concentration (Schwalenberg et al., 2010). Values of parameter m from 1.76 to 2 are generally used in continental margins (e.g. Edwards, 1997; Ghosh et al., 2006; Guerin and Goldberg, 2002; Hyndman et al., 1999; Lee and Collett, 2008; Lu and McMechan, 2002; Reister, 2003; Riedel et al., 2006; Weitemeyer et al., 2006). The value of the parameter n depends somewhat on sediment grain size and the gas hydrate saturation (Spangenberg, 2001).

As shown in Fig. 10, the background apparent porosity is ~62% around the pockmark in profile C12. However, the apparent porosity is down to ~52% near the pockmark. If we use m (=n) = 1.8, the

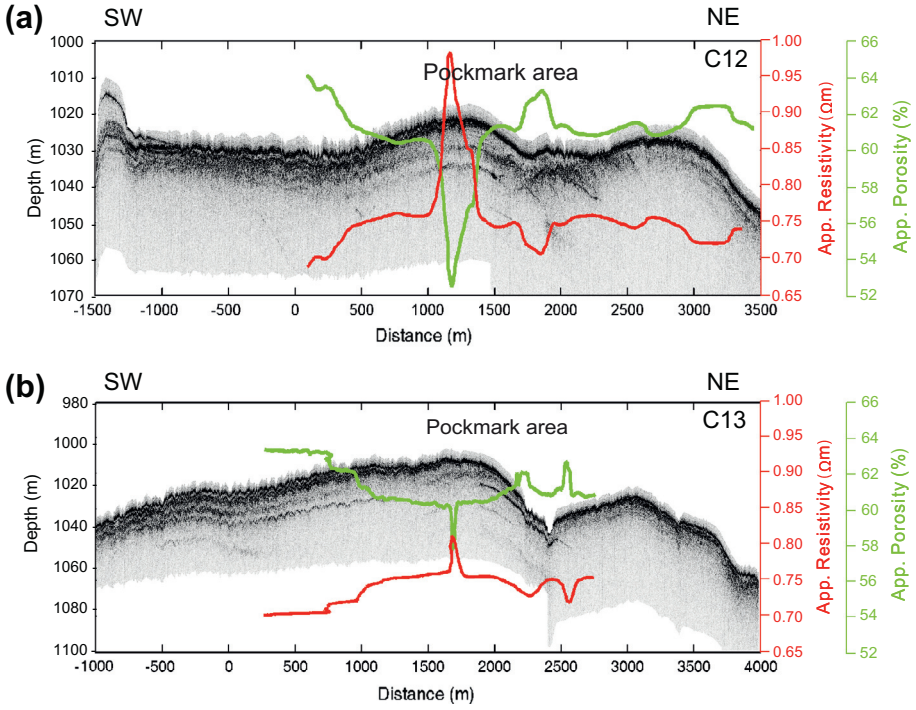

Fig. 10. Comparison between apparent resistivity or apparent porosity values and sub-bottom profiler images along profiles C12 (a) and C13 (b), respectively. It is noted that the ~8% low porosity anomaly occur around the pockmark area. However, the resistivity or porosity anomaly occurs mainly beneath the uplifted flank in the SW of the pockmark, instead of in the middle of the pockmark. The pockmark itself shows a slightly low resistivity anomaly.

10% porosity anomaly may be due to the gas hydrate replacement. That is, the gas hydrate saturation is about 16% in the shallow sediments below the pockmark. However, if the location of profile C12 does not meet the pressure–temperature condition for the formation of gas hydrate, the explanation of the porosity anomaly could be also due to carbonates, similar to in region A.

5. Conclusions

We have conducted the first survey of the seabed resistivity off SW Taiwan. The results show that the marine resistivity survey is a promising technique to describe seafloor characteristics. Our MCSEM results show high resistivity anomaly at gas seep site G96 (area A), at the pockmark in area C. At gas seep site G96, the high resistivity anomaly may be due to the existence of authigenic carbonates, because it may be difficult to form the crystallized gas hydrates in the shallow water in area A. In contrast, the high resistivity anomaly at the pockmark in area C may suggest the existence of gas hydrate in the shallow seabed. Overall, there is suitable condition of high pressure and low temperature in areas B and C for crystallized gas hydrate. If we ascribe the resistivity anomaly to the existence of gas hydrates below the pockmark in profile C12, the gas hydrate saturation is about 16% in the shallow sediments.

Acknowledgements

This research was mainly supported from the Central Geological Survey of the Ministry of Economic Affairs, Taiwan, and the National Science Council, Taiwan. We appreciate the crew of R/V OR1 who helped collect data during the cruise OR1-931. We also appreciate both Mrs. Matthew Gould and John Bailey for assistance in operating the towed EM system during the cruise. We acknowledge Prof. Chien-Chih Chen for a fruitful discussion and Dr. Wen-Bin Doo for preparing some figures.

References

Archie, G.E., 1942. The electrical resistivity log as an aid in determining some reservoir characteristics. Pet. Trans. AIME 146, 54–62.
Butterworth, S., 1930. On the theory of filter amplifiers. Exp. Wireless Wireless Eng. 7, 536–541.
Chen, S.-C., Hsu, S.-K., Tsai, C.-H., Ku, C.-Y., Yeh, Y.-C., Wang, Y., 2010. Gas seepage, pockmarks and mud volcanoes in the near shore of SW Taiwan. Mar. Geophys. Res. 31, 133–147.
Chi, W.-C., Reed, D.L., Liu, C.-S., Lundberg, N., 1998. Distribution of the bottom-simulating reflector in the offshore Taiwan collision zone. Terr. Atmos. Ocean. Sci. 9, 779–794.
Chiang, C.-W., Goto, T., Chen, C.-C., Hsu, S.-K., 2011. Efficiency of a marine towed electrical resistivity method. Terr. Atmos. Ocean. Sci. 22, 443–446.
Chiang, C.-W., Goto, T., Mikada, H., Chen, C.-C., Hsu, S.-K., 2012. Sensitivity of deep-towed marine electrical resistivity tomography by using two-dimensional inversion: a case study of methane hydrate. Terr. Atmos. Ocean. Sci. 23 (6), 725–732.
Chuang, P.C., Yang, T.F., Lin, S., Lee, H.F., Lan, T.F., Hong, W.L., Liu, C.S., Chen, J.C., Wang, Y., 2006. Extremely high methane concentration in bottom water and cored sediments from offshore southwestern Taiwan. Terr. Atmos. Ocean. Sci. 17, 903–920.
Edwards, R.N., 1997. On the resource evaluation of marine gas hydrate deposits using sea-floor transient electric dipole–dipole methods. Geophysics 62, 63–74.
Ellis, M., Evans, R.L., Hutchinson, D., Hart, P., Gardner, J., Hagen, R., 2008. Electromagnetic surveying of seafloor mounds in the gulf of Mexico. Mar. Pet. Geol. http://dx.doi.org/10.1016/j.marpetgeo.2007.12.006.
Evans, R.L., 2001. Measuring the shallow porosity structure of sediments on the continental shelf: a comparison of an electromagnetic approach with cores and acoustic backscatter. J. Geophys. Res. 106 (C11), 27047–27060.
Evans, R.L., 2007. Using CSEM techniques to map the shallow section of seafloor: from the coastline to the edges of the continental slope. Geophysics 72, 105–116.
Evans, R.L., Lizarralde, D., 2011. The competing impacts of geology and groundwater on electrical resistivity around Wrightsville Beach, N.C. Cont. Shelf Res. 31, 841–848.
Evans, R.L., Law, L.K., St Louis, B., Cheesman, S., Sananikone, K., 1999. The shallow porosity structure of the Eel shelf, northern California results of a towed electromagnetic survey. Mar. Geol. 154, 211–226.
Ghosh, R., Sain, M.K., Thakur, N.K., 2006. Physical parameters of hydrated sediments estimated from marine seismic reflection data. Curr. Sci. 90, 1421–1430.
Goto, T.N., Kasaya, T., Machiyama, H., Takagi, R., Matsumoto, R., Okuda, Y., Kinoshita, M., 2008. A marine deep-towed DC resistivity survey in a methane hydrate area, Japan Sea. Explor. Geophys. 39 (1), 52–59.
Guerin, G., Goldberg, D., 2002. Sonic waveform attenuation in gas hydrate-bearing sediments from the Mallik 2L–38 research well, Mackenzie Delta, Canada. J. Geophys. Res. 107, 2088.

Hoefel, F., Evans, R.L., 2001. Impact of low salinity porewater on seafloor electromagnetic data: a means of detecting submarine groundwater discharge? Estuar. Coast. Shelf Sci. 52, 179–189.

Hovland, M., Judd, A., 1988. Seabed Pockmarks and Seepages: Impact on Geology, Biology, and the Marine Environment. Springer.

Hovland, M., Judd, A.G., Burke Jr., R.A., 1993. The global flux of methane from shallow submarine sediments. Chemosphere 26 (1), 559–578.

Hsu, S.-K., Wang, S.-Y., Liao, Y.-C., Yang, T.F., Jan, S., Lin, J.-Y., Chen, S.-C., 2013. Tide-modulated gas emissions and tremors off SW Taiwan, Earth Planet. Sci. Lett. 369–370, 98–107.

Hyndman, R.D., Yuan, T., Moran, K., 1999. The concentration of deep sea gas hydrates from downhole electrical resistivity logs and laboratory data. Earth Planet. Sci. Lett. 172, 167–177.

Jackson, P.D., Smith, D.T., Stanford, P.N., 1978. Resistivity-porosity-particle shape relationships for marine sands. Geophysics 43, 1250–1268.

Jiang, W.-T., Chen, J.-C., Huang, B.-J., Chen, C.-J., Lee, Y.-T., Huang, P.-R., Lung, C.-C., Huang, S.-W., 2006. Mineralogy and physical properties of cored sediments from the gas hydrate potential area of offshore southwestern Taiwan. Terr. Atmos. Ocean. Sci. 17, 981–1007.

Lee, M.W., Collett, T.S., 2008. Integrated analysis of well logs and seismic data to estimate gas hydrate concentrations at Keathley Canyon, Gulf of Mexico. Mar. Pet. Geol. 25 (9), 924–931.

Lin, A.T., 2010. Investigation and evaluation of gas hydrate resources in the offshore area of southwestern Taiwan: seismic and heat flow studies (3/4) – Gas hydrate-bearing sedimentary strata structures and sedimentation characters. Central Geological Survey, MOEA Taiwan Report 99–25-F, 102 p. (in Chinese).

Lin, S., Hsieh, W.-C., Lim, Y.C., Yang, T.F., Liu, C.-S., Wang, Y., 2006. Methane migration and its influence on sulfate reduction in the Good Weather Ridge region, South China Sea continental margin sediments. Terr. Atmos. Ocean. Sci. 17, 883–902.

Liu, C.-S., Huang, I.L., Teng, L.S., 1997. Structural features off southwestern Taiwan. Mar. Geol. 137, 305–319.

Liu, C.-S., Deffontaines, B., Lu, C.-Y., Lallemand, S., 2004. Deformation patterns of an accretionary wedge in the transition zone from subduction to collision offshore southwestern Taiwan. Mar. Geophys. Res. 25, 123–137.

Liu, C.-S., Schnurle, P., Wang, Y., Chung, S.-H., Chen, S.-C., Hsiuan, T.-H., 2006. Distribution and characters of gas hydrate offshore of southwestern Taiwan. Terr. Atmos. Ocean. Sci. 17, 615–644.

Lu, S., McMechan, G.A., 2002. Estimating of gas hydrate and free gas saturation, concentration, and distribution from seismic data. Geophysics 67, 582–593.

Milkov, A.V., 2000. Worldwide distribution of submarine mud volcanoes and associated gas hydrates. Mar. Geol. 167, 29–42.

Paull, C.K., Ussler III, W., 2001. History and significance of gas sampling during DSDP and ODP drilling associated with gas hydrates. Nat. Gas Hydrates: Occurrence, Distrib., Detect. 124, 53–65.

Reister, D.B., 2003. Using measured velocity to estimate gas hydrate concentration. Geophysics 68, 884–891.

Riedel, M., Long, P.E., Collett, T.S., 2006. Estimates of in situ gas hydrate concentration from resistivity monitoring of gas hydrate bearing sediments during temperature equilibration. Mar. Geol. 227, 215–225.

Schwalenberg, K., Haeckel, M., Poort, J., Jegen, M., 2010. Evaluation of gas hydrate deposits in an active seep area using marine controlled source electromagnetics: results from Opouawe Bank, Hikurangi Margin, New Zealand. Mar. Geol. 272, 79–88.

Sibuet, J.-C., Hsu, S.-K., 2004. How was Taiwan created? Tectonophysics 379, 159–181.

Spangenberg, E., 2001. Modeling of the influence of gas hydrate content on the electrical properties of porous sediments. J. Geophys. Res. 106, 6535–6548.

Weitemeyer, K.A., Constable, S.C., Key, K.W., Behrens, J.P., 2006. First results from a marine controlled-source electromagnetic survey to detect gas hydrates offshore Oregon. Geophys. Res. Lett. 33, L03304.

Weitemeyer, K.A., Constable, S., Trehu, A.M., 2011. A marine electromagnetic survey to detect gas hydrate at Hydrate Ridge. Oregon. Geophys. J. Int. 187 (45), 45.

Xu, W., Ruppel, C., 1999. Predicting the occurrence, distribution, and evolution of methane gas hydrate in porous marine sediments. J. Geophys. Res. 104 (B3), 5081–5095. http://dx.doi.org/10.1029/1998JB900092.